The effects of postdeposition annealing conditions on structure and created defects in $Zn_{0.90}Co_{0.10}O$ thin films deposited on Si(100) substrate

Musa Mutlu Can[a)]
Faculty of Engineering and Natural Sciences, Sabancı University, Tuzla 34956, İstanbul, Turkey; and Nanotechnology Research and Application Center (SUNUM), Sabancı University, Tuzla 34956, İstanbul, Turkey

Tezer Fırat
Department of Physics Engineering, Hacettepe University, 06800 Beytepe, Ankara, Turkey

S.Ismat Shah
Department of Material Science and Engineering, Department of Physics and Astronomy, University of Delaware, Newark, Delaware 19716

Feray Bakan and Ahmet Oral
Faculty of Engineering and Natural Sciences, Sabancı University, Tuzla 34956, İstanbul, Turkey; and Nanotechnology Research and Application Center (SUNUM), Sabancı University, Tuzla 34956, İstanbul, Turkey

(Received 31 July 2012; accepted 3 December 2012)

We analyze the effect of postdeposition annealing conditions on both the structure and the created defects in $Zn_{0.90}Co_{0.10}O$ thin films, which deposited on the Si(100) substrates by the radio frequency magnetron sputtering technique using a homemade target. The dependence of the number and distribution of defects in homogeneously substituted Co^{+2} for Zn^{+2} ions in ZnO lattice on the annealing conditions is investigated. Orientations of thin films are in the [0002] direction with a surface roughness changing from 67 ± 2 nm to 25.8 ± 0.6 nm by annealing. The Co^{+2} ion substitution, changing from 7.5% ± 0.3% to 8.8 ± 0.3%, leads to the formation of Zn–O–Co bonds instead of Zn–O–Zn bonds and splitting of the Co 2*p* energy level to Co $2p_{1/2}$ and Co $2p_{3/2}$ with an energy difference of 15.67 ± 0.06 eV. The defects in the lattice are revealed from the correlations between Zn–O–Co bonds and intensity of the Raman peak at around 691 cm^{-1}. In addition, the asymmetry changes of O 1*s* peak positions in the x-ray photoelectron spectra are in agreement with the Raman results.

I. INTRODUCTION

ZnO is one of the most widely investigated oxide semiconductors because of the room temperature magnetic applications.[1–3] Numerous theoretical and experimental studies have been performed on transition metal-doped ZnO to understand the mechanisms of ferromagnetism.[4–13] Nevertheless, the origin of magnetic behavior of transition metal-doped ZnO structure[4–13] is still not well understood. There are three main suggestions for the magnetic behavior in doped ZnO. The first one is the *p–d* hybridization of orbitals due to holes in the lattice.[5,6] The second one is the *s–d* hybridization in the n-type semiconductor,[7] and the third potential mechanism is the formation of transition metal clusters[6,8,10,14] or the secondary phases in the ZnO lattice.[14,15] These results have actually increased the debate on the magnetic properties of ZnO, rather than giving a definite answer. Nowadays, another suggestion is focused on the shallow donor/acceptor levels originating from defects in the ZnO crystal.[16,17] Recent findings have shown the importance of defects, in addition to transition atoms in lattice, on the ferromagnetic ordering.[18–22] Coey et al.[22] emphasized the magnetic formation without magnetic ions in both d^0 systems and other oxides with crystal defects.The point defects also determine the electrical and optical properties of ZnO thin films.[23–28] Furthermore, the point defect density of ZnO is studied for the optical performance,[29] photoelectrode application for the solar cells,[30] carrier relaxation dynamics,[31] gas sensing,[32] and fluorescent properties for biomedical applications.[33] The defects are seen as the main control mechanism of physical properties of ZnO. Sol–gel,[34] molecular beam epitaxy,[35] pulsed laser deposition,[36] metal organic chemical vapor deposition,[37] and the radio frequency (RF) magnetron sputtering[38] techniques are widely used to grow ZnO thin films. The amount of defects in a thin film can be controlled by changing the specific parameters used in the deposition technique. Main control parameters are the gases and their partial pressures used in the sputter deposition, as well as postdeposition annealing temperature and conditions.[34–38]

Most of the studies are concentrated on "Zn-rich" defects, the oxygen vacancies, and interstitial Zn atoms, due to their lower enthalpy of formation in the ZnO lattice.[39] The annealing temperature and deposition/postdeposition atmosphere are seen as the main parameters to form and

[a)]Address all correspondence to this author.
e-mail: musamutlucan@gmail.com
DOI: 10.1557/jmr.2012.422

control the point defects in the lattice.[23,26,28,40] There have been quite a few systematic analyses on defect formation and relation of these defects with dopant atoms, such as transition metals or nonmagnetic elements, in the lattice. In addition to the effects of transition metals substitution for host anion atoms in lattice, the point defects are also effective on the physical properties, such as ferromagnetic behavior,[41,42] optical transitions,[25–27] and electrical properties[26] due to the formation of shallow energy levels.

In this study, we have investigated the optimum growth and annealing conditions of the RF magnetron sputtered $Zn_{0.90}Co_{0.10}O$ thin films, deposited on Si(100) substrates. This work is focused on obtaining homogeneously distributed Co dopant atoms and point defects in the $Zn_{0.90}Co_{0.10}O$ thin films by controlling growth and postdeposition annealing conditions. We also aim to assist future studies on the point defects to control physical properties of ZnO.

II. EXPERIMENTAL

We performed the $Zn_{0.90}Co_{0.10}O$ deposition in a RF magnetron sputtering system equipped with 2″ sputter guns. The thin films were deposited from homemade $Zn_{0.90}Co_{0.10}O$ targets. The synthesis process of the homemade targets was described in a previous study.[43,44] The targets also exhibited 0.7–1.1% tungsten contamination, which is generated from the vial and the balls of the mechanical miller during the synthesis process.[43]

10×10 mm Si(100) single crystal samples were used as substrates after cleaning in acetone/alcohol and they were attached to the specimen holder by silver paste. The depositions were performed in argon (70%)–oxygen (30%) plasma for 60 min at 100 W RF power under 10 mTorr pressure. During the depositions, the sample holder temperature was kept at 420 ± 1 °C. This specific gas concentration was the optimal condition of pure ZnO growth in our earlier work,[26] where we varied the partial pressures from 0:100 to 50:50 percent. Furthermore, this concentration is optimal to eliminate the formation of metallic Zn clusters and obtain large grain sizes with the preferred orientations.

To create defects in the lattice, three different postdeposition annealing conditions were used. One type of samples was deposited without postdeposition annealing, and the others were deposited with postdeposition annealing under vacuum (in pressure range of 5×10^{-7} to 1×10^{-6} Torr) and under 1 mTorr of O_2 atmosphere.

The structural analyses were performed by x-ray diffraction (XRD). The XRD patterns were obtained in the 2θ ranges of 15° to 80° using a Rigaku Dmax B model diffractometer (Rigaku, Tokyo, Japan) by using Cu K_α radiation source with a scanning speed of 0.02°/min. Chemical analyses of the films were performed by Oxford Instruments PentaFET-6900 model energy-dispersive x-ray spectrometer (EDS) (Oxford Instruments, Oxford, UK) under 5 kV acceleration voltages.

The surface morphology of the films was examined by JEOL/JMS-7400F model scanning electron microscopy (SEM) (JEOL USA Inc., Peabody, MA) under 3 kV potential.

X-ray photoelectron spectra (XPS) spectra were obtained in a VG ESCALAB 220i-XL (Thermo VG Scientific Ltd., West Sussex, UK) equipped with Al K_α monochromatic x-ray radiation source and solid state imaging detector with ~0.1 eV resolution. All measurements with XPS were done under $\sim 1 \times 10^{-9}$ Torr pressure. The analyses were done by fixing C 1s binding energy level at 284.6 eV.

The room temperature micro-Raman measurements were taken in the backscattering geometry using a Renishaw inVia Reflex Model Raman spectrometer (Renishaw, Gloucestershire, UK). A 514 nm Ar laser line, with spot diameter of ~2 μm, was used for excitation. The measurements were recorded in 100–1500 cm^{-1} and in 550–750 cm^{-1} range.

Atomic force microscope (AFM) data were acquired in tapping mode with an AFM from NanoMagnetics Instruments, Ltd. (Oxford, UK), using NCHAu-D cantilevers with sharp tips, $k \sim 40$ N/m and $f_0 \sim 300$ kHz.

III. RESULTS AND DISCUSSION

The XRD patterns were measured in wide 2θ range from 15° to 80° to detect the existence of all the possible crystal phases, in addition to ZnO. The peak positions of Si(100) substrate are also demonstrated in Fig. 1, in addition to the

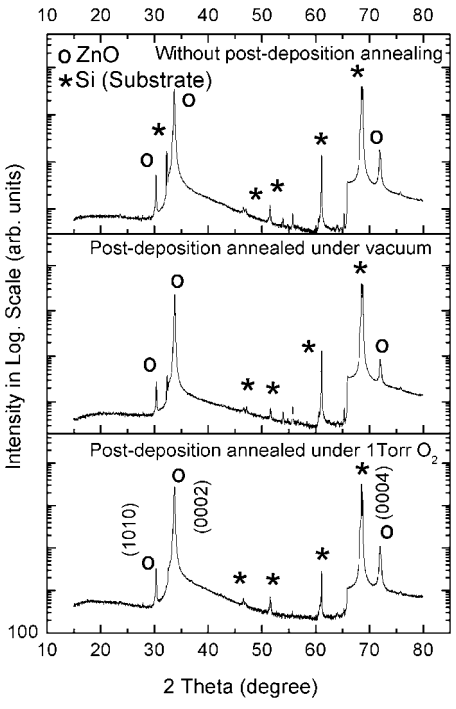

FIG. 1. XRD patterns of the films grown from $Zn_{0.90}Co_{0.10}O$ target without postdeposition annealing, postdeposition annealing under vacuum atmosphere, and postdeposition annealing under 1 Torr O_2 atmosphere.

XRD peaks of the ZnO thin films. The spectra plotted in logarithmic scale to identify the extra peaks. It was found that there are three main peaks in the spectra at around 30.32°, 33.84°, and 72.02°. These peaks were in agreement with the planes of (1010), (0002), and (0004) of the hexagonal ZnO (ICDD PDF No. 00-036-1451), respectively. The dominant peak was observed for the (0002) plane, showing the preferred growth direction. No peaks from metallic Co or oxide state of Co were observed, which can be correlated to the clustering of the Co atoms in the ZnO lattice.

The XRD patterns were not sufficient to draw out information about the amount of Co and other impurity atoms in ZnO. The concentration of Co and the other contaminant atoms in the films were measured from the EDS spectra. The EDS data, shown in Table I, are the results of the mean values of five different regions of the sample. All the data, shown in Table I, are normalized by the total number of atoms in the lattice; Zn, Co, W, and O. The average concentration of tungsten atoms in the films was 0.9% ± 0.1%. The Co distributions on the surface of

TABLE I. EDS data of $Zn_{0.90}Co_{0.10}O$ thin films.

Postdeposition annealing conditions	Normalized atomic ratio of Zn (%)	Normalized atomic ratio of Co (%)	Normalized atomic ratio of W (%)	Thickness(nm)
Without postannealing	41.1 ± 0.5	8.8 ± 0.2	0.9 ± 0.1	962 ± 4
Under vacuum (in pressure range of 5×10^{-7} and 1×10^{-6} Torr)	41.5 ± 1.7	7.5 ± 0.3	1.1 ± 0.2	707 ± 1
Under 1 Torr O_2	42.1 ± 1.2	8.3 ± 0.2	0.7 ± 0.1	853 ± 5

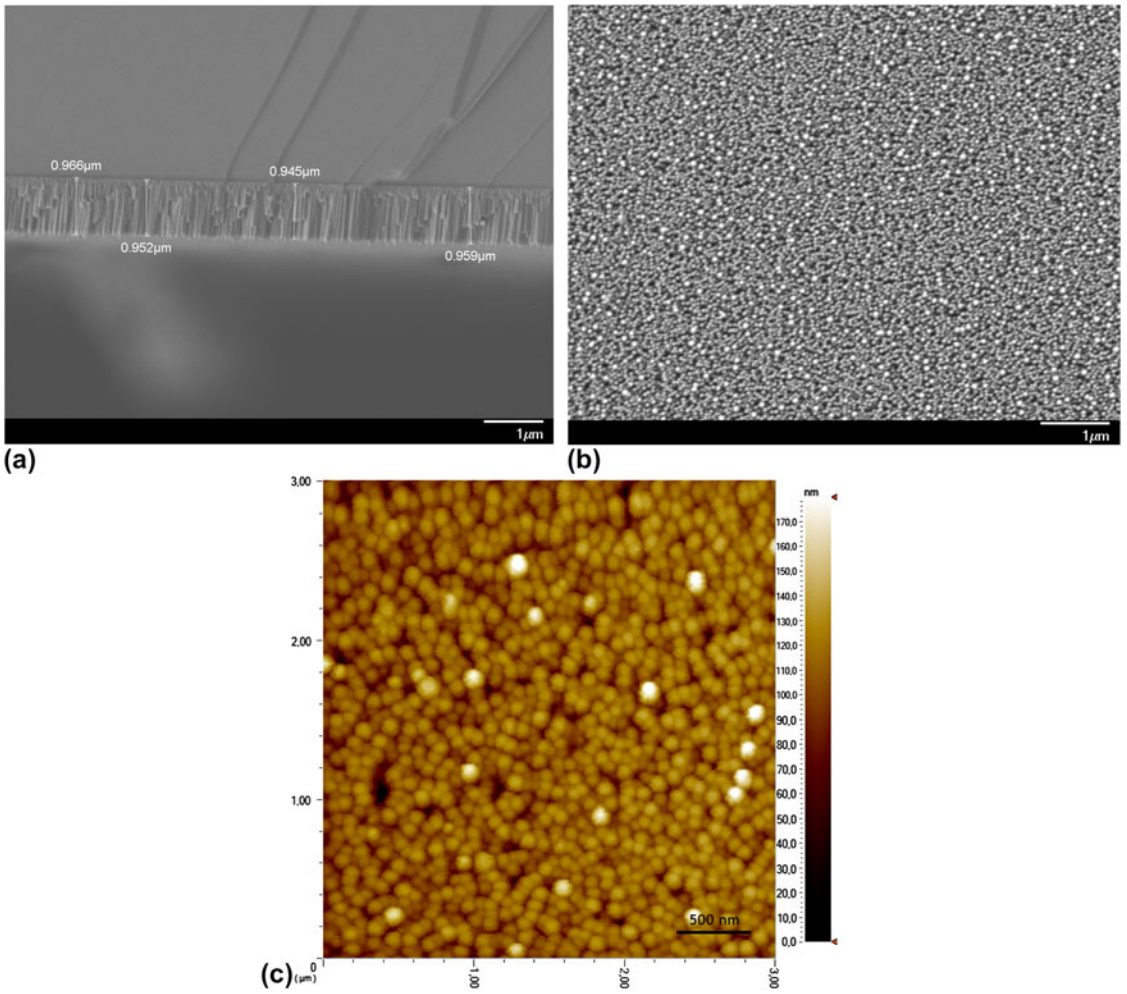

FIG. 2. The SEM micrographs of (a) cross-sectional thickness and (b) surface morphology and (c) the AFM image of $Zn_{0.9}Co_{0.1}O$ films without postdeposition annealing.

the $Zn_{0.90}Co_{0.10}O$ thin films were 8.2% ± 0.3%. The homogeneity in each thin film did not vary considerably. As it was mentioned in Sec. II, the tungsten impurities were suspected to come from the manufacturing process of the target.

The cross-sectional measurements were performed using SEM to determine the thickness of the films that were grown from $Zn_{0.90}Co_{0.10}O$ targets. The results are summarized in Table I. The cross-sectional SEM image of the thin film deposited without the postdeposition annealing is given in Fig. 2(a). Morphologically, the only change observed is the surface roughness, measured by SEM[45] and AFM, at different postdeposition annealing conditions. The SEM and AFM images of the thin films without the postdeposition are shown in Figs. 2(b) and 2(c), respectively. The AFM images were in agreement with the SEM data. The AFM images were used to measure the surface roughness. The measured roughness shows that the postdeposition annealing procedure decreases the surface roughness. The surface roughness, calculated from AFM images, were 67 ± 2 nm, 37.2 ± 0.5 nm, and 25.8 ± 0.6 nm for the non-postdeposition annealing, annealing under vacuum, and annealing under O_2 conditions, respectively. The main reason of decline in roughness originates from the enhanced grains by annealed in vacuum atmosphere and oxygen.[46–49] Annealing at 400 °C seems to supply sufficient energy to surface atoms to diffuse into the surface vacancies or defects.[48] The smaller surface roughness at thin film annealed in an oxygen environment also reveals larger grain size than the others due to an adequate amount of oxygen atoms in environment.

After proving the existence of Co atoms in films, their positions in the lattice were determined by the XPS spectra. The spectra of the thin films are presented in Fig. 3. The energy levels of Zn, Co, and O were clearly observed in the spectra. The postdeposition annealing conditions, doped Co atoms, or W impurities did not change the position of the energy levels of Zn $2p_{1/2}$ and Zn $2p_{3/2}$, which are 1020.41 and 1043.48 eV, respectively. The data shown are the mean values of all thin films. The energy difference between Zn $2p_{1/2}$ and Zn $2p_{3/2}$ was calculated to be 23.07 ± 0.02 eV, which was in agreement with the literature.[50]

The Co 2*p* and O 1*s* XPS peaks were investigated in detail to understand the positions of Co atoms and O vacancies in lattice, respectively.[51–55] The Co 2*p* peak energy splits into two singlets as shown in Figs. 4(a)–4(c). As seen from figure, the energy split, 15.67 ± 0.06 eV, between Co $2p_{3/2}$ and Co $2p_{1/2}$ states is the same for all the films. Furthermore, the energy shift of the Co $2p_{1/2}$ peak, with respect to the metallic state of cobalt (778.1–778.3 eV[50]), is 780.05 ± 0.04 eV. We interpret this as the cobalt atoms have substituted Zn^{+2} ions as Co^{+2}, as mentioned in previous studies.[7,50]

The XPS is a surface sensitive tool and can only give information about 20 nm depths from the surface. However,

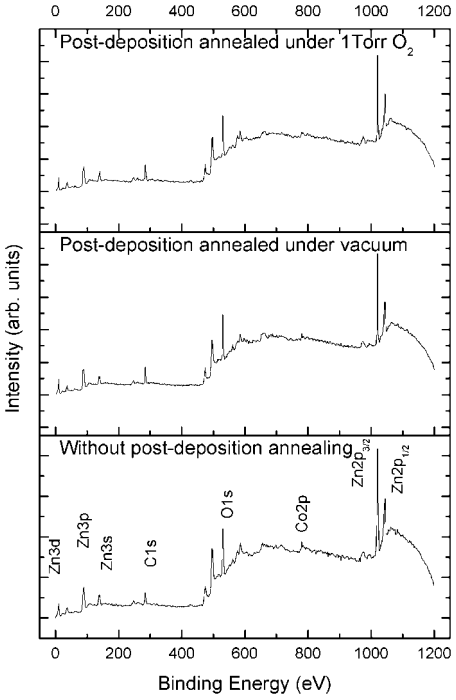

FIG. 3. XPS spectra of the films grown from $Zn_{0.90}Co_{0.10}O$ target without the postdeposition annealing, postdeposition annealing under vacuum atmosphere, and postdeposition annealing under 1 Torr O_2 atmosphere.

if the surface of the film is not too different than the rest and is not effected by other factors, the XPS data can be taken as representative of the film itself. Furthermore, the XPS may also provide general information about the point defects density in thin films. The effects of the postdeposition annealing condition on the defects were also investigated by analyzing O 1*s* peaks in XPS data. The oxygen 1*s* peak observed in XPS is composed of three closely spaced energy levels: O_a, O_b, and O_c. The analyses were done for spectra taken under identical conditions, and the defect density was related to the change at the ratios of relative intensities in O 1*s* energy level. The O 1*s* energy levels in Fig. 4 were fitted to three curves, mixture of the Gaussian and Lorentzian functions. The calculated average values of the peak positions are at around 529.6 ± 0.1 eV (O_a), 530.5 ± 0.1 eV (O_b), and 531.6 ± 0.1 eV (O_c) as presented in Table II.

O_a, O_b, and O_c peak positions are originated from the O^{-2} ions surrounded by Zn atoms, from defects either having or originating O^{-2} deficiency in lattice and from chemisorbed dissociated oxygen or OH species on the surface as H_2O molecules or weakly bonded CO_3 molecules, respectively.[51,52] The postdeposition annealing conditions did not shift the energy level. Nevertheless, a change in relative intensities of the normalized areas of A_a (the area of O_a peak), A_b (the area of O_b peak), and A_c (the area of O_c peak) were observed at different annealing conditions. In the analysis, $A_a/(A_a + A_b)$ and $A_b/(A_a + A_b)$ ratios were investigated, relating to A_a and A_b to the amount of O^{-2} cation in the lattice. The results of the

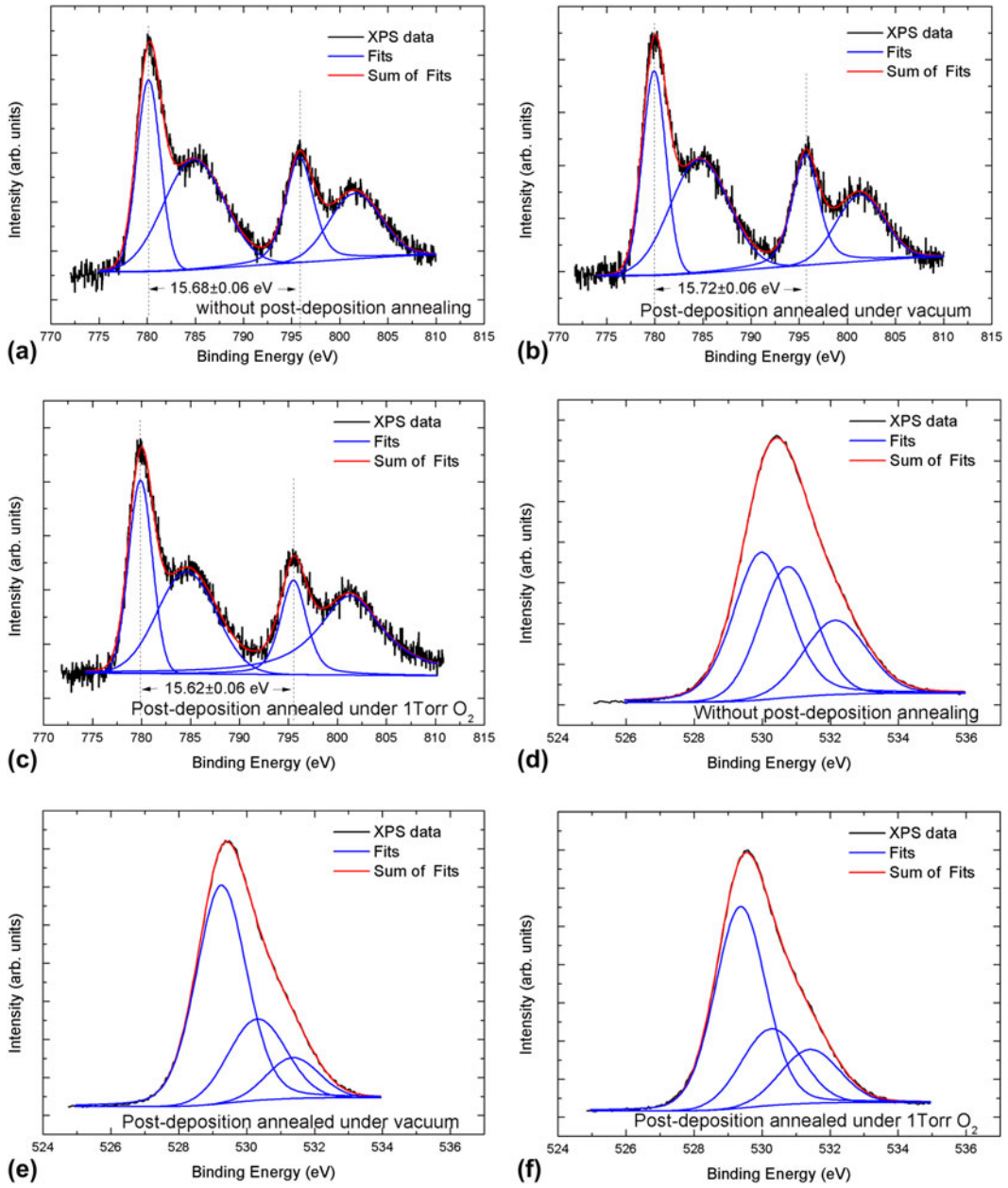

FIG. 4. XPS spectra of (a)–(c) the Co 2*p* (in binding energy range of 770 and 815 eV) and (d)–(f) O 1*s* (in binding energy range of 524 and 537 eV) energy levels for the films deposited by $Zn_{0.90}Co_{0.10}O$ target without postdeposition annealing, postdeposition annealing under vacuum, and postdeposition annealing under 1 Torr O_2 atmosphere, respectively.

calculations were shown in Table II. With postdeposition annealing, the intensity in $A_b/(A_a + A_b)$ ratios decreased, while that in $A_a/(A_a + A_b)$, ratios increased. This suggests that the postdeposition annealing causes lower defect density due to O^{-2} deficiency in the main ZnO lattice. The changes in ratios are demonstrated in Table II.

The possible defects in the lattice due to cobalt substitution and postdeposition annealing were also analyzed using Raman spectra as shown in Fig. 5. The measurements were taken in 100–1500 cm^{-1} and 550–750 cm^{-1} Raman shift range as shown in Fig. 5(a) and in Fig. 5(b), respectively. In addition to the Raman peaks of silicon substrate at 298 cm^{-1},[56] 520 cm^{-1},[57] and 618 cm^{-1},[56,57] five more modes (a broad mode in between 200–280, 437 cm^{-1}, another broad peak in between 630–760, 942 and 986 cm^{-1}) were obtained in the Raman spectra. Two of these broad peaks, the peak in between 200 and 280 cm^{-1} and the peak at around 437 cm^{-1}, are attributed to the ZnO vibration modes.[56] Furthermore, the broad peaks around 942 and 986 cm^{-1} were observed as the second-order vibrations of ZnO crystal.[57] The last Raman mode was at 691 cm^{-1} as shown on Fig. 5(b). This mode was related to

TABLE II. Fitted curves of O 1*s* peak positions for thin films deposited from $Zn_{0.90}Co_{0.10}O$ target.

Postdeposition annealing conditions	O_a (eV)	O_b (eV)	O_c (eV)	$(A_a/A_a + A_b) \times 100$	$(A_b/A_a + A_b) \times 100$
Without postannealing	530.0 ± 0.1	530.8 ± 0.1	532.1 ± 0.1	56	44
Under vacuum (in pressure range of 5×10^{-7} and 1×10^{-6} Torr)	529.3 ± 0.1	530.3 ± 0.1	531.4 ± 0.1	71	29
Under 1 Torr O_2	529.4 ± 0.1	530.3 ± 0.1	531.4 ± 0.1	72	28

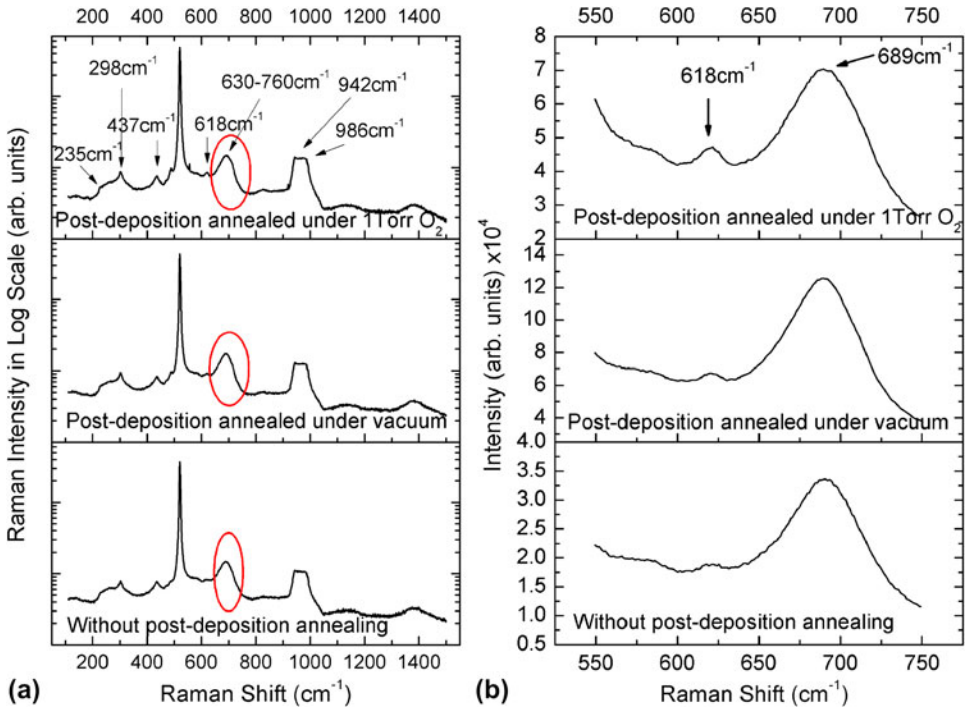

FIG. 5. The Raman spectra of thin films grown without postdeposition annealing, postdeposition annealing under vacuum, and postdeposition annealing under 1 Torr O_2 atmosphere (a) in the full range and (b) in the interval of 550–750 cm^{-1}.

the disordered Zn–O–Co vibrations.[58] The analysis was extended by repeating the measurements in between 550 and 750 cm^{-1} for 300 s integration time to make the peaks more visible. A specific enhancement in intensity depending on postdeposition annealing was observed.

The study of Sudakar et al.[58] emphasized the disappearance of Zn–O–Co vibrations by forming oxygen vacancies at around Co atoms in the lattice, and the consequences were observed by the decreased Raman intensity, which was in agreement with our observations, as shown in Fig. 5(b). The decrease in this peak intensity in Raman spectrum is attributed to the decrease in the concentration of oxygen-dependent defects in the lattice. The lowest intensity was observed in the film deposited without postdeposition annealing that means the highest defects according to the others.

IV. CONCLUSIONS

In this study, the $Zn_{0.90}Co_{0.10}O$ thin films were grown by using RF sputtering with homemade $Zn_{0.90}Co_{0.10}O$ targets. It was attempted to dope 10% Co atoms in ZnO films by using $Zn_{0.90}Co_{0.10}O$ target; however, only 8.2% ± 0.3% Co atoms were evenly distributed as determined from the results of surface analysis. The Co atoms were observed to be substituting the Zn atoms in lattice, and this also decreased the band gap at around 0.34 eV, according to the XPS spectra. In addition, the concentrations of tungsten impurities in thin films were in between 0.5% ± 0.1% and 1.1% ± 0.2% and these impurities located as oxidized states. In addition to the expected structure, the defects were also formed in the lattice, which was found from the asymmetry of O 1*s* peak positions and from the intensity decrease of Raman mode at around 691 cm^{-1}.

ACKNOWLEDGMENTS

We acknowledge the financial support of the Scientific and Technological Research Council of Turkey (TUBİTAK), BİDEB-2218 program.

REFERENCES

1. T. Fukumura, Y. Yamada, H. Toyosaki, T. Hasegawa, H. Koinuma, and M. Kawasaki: Exploration of oxide-based diluted magnetic semiconductors toward transparent spintronics. *Appl. Surf. Sci.* **223**, 62–67 (2004).
2. C.B. Fitzgerald, M. Venkatesan, L.S. Dorneles, R. Gunning, P. Stamenov, J.M.D. Coey, P.A. Stampe, R.J. Kennedy, E.C. Moreira, and U.S. Sias: Magnetism in dilute magnetic oxide thin films based on SnO_2. *Phys. Rev. B* **74**, 115307 (2006).
3. M.J. Calderon and S. Das Sarma: Theory of carrier mediated ferromagnetism in dilute magnetic oxides. *Ann. Phys.* **322**, 2618–2634 (2007).
4. F. Matsukura, H. Ohno, and T. Dietl: In *Handbook of Magnetic Materials*, edited by K.H.J. Buschow (Elsevier Science, Amsterdam, Netherlands, 2002).
5. S.J. Pearton, W.H. Heo, M. Ivill, D.P. Norton, and T. Steiner: Dilute magnetic semiconducting oxides. *Semicond. Sci. Technol.* **19**, R59–R74 (2004).
6. A.S. Risbud, N.A. Spaldin, Z.Q. Chen, S. Stemmer, and R. Seshadri: Magnetism in polycrystalline cobalt-substituted zinc oxide. *Phys. Rev. B* **68**, 205202 (2003).
7. Y.Z. Peng, T. Liew, W.D. Song, C.W. An, K.L. Teo, and T.C. Chong: Structural and optical properties of Co-doped ZnO thin film. *J. Supercond.* **18**(1), 97–103 (2005).
8. J.H. Park, M.G. Kim, H.M. Jang, S. Ryu, and Y.M. Kim: Co-metal clustering as the origin of ferromagnetism in Co-doped ZnO thin films. *Appl. Phys. Lett.* **84**(8), 1338–1340 (2004).
9. D.P. Norton, M.E. Overberg, S.J. Pearton, K. Pruessner, J.D. Budai, L.A. Boatner, M.F. Chisholm, J.S. Lee, Z.G. Khim, Y.D. Park, and R.G. Wilson: Ferromagnetism in cobalt-implanted ZnO. *Appl. Phys. Lett.* **83**(26), 5488–5490 (2003).
10. P. Sati, R. Hayn, R. Kuzian, S. Regnier, S. Schafer, A. Stepanov, C. Morhain, C. Deparis, M. Laugt, M. Goiran, and Z. Golacki: Magnetic Anisotropy of Co^{2+} as Signature of Intrinsic Ferromagnetism in ZnO:Co. *Phys. Rev. Lett.* **96**, 017203 (2003).
11. M. Naeem, S.K. Hasanain, M. Kobayashi, Y. Ishida, A. Fujimori, S. Buzby, and S.I. Shah: Effect of reducing atmosphere on the magnetism of $Zn_{1-x}Co_xO$ ($0 \leq x \leq 0.10$) nanoparticles. *Nanotechnology* **17**, 2675–2680 (2006).
12. J. Hays, K.M. Reddy, N.Y. Graces, M.H. Engelhard, V. Shutthanandan, M. Luo, C. Xu, N.C. Giles, C. Wang, S. Thevuthasan, and A. Punnoose: Effect of Co doping on the structural, optical and magnetic properties of ZnO nanoparticles. *J. Phys. Condens. Matter* **19**, 266203 (2007).
13. C.B. Fitzgerald, M. Venkatesan, J.G. Lunney, L.S. Dorneles, and J.M.D. Coey: Cobalt-doped ZnO–a room temperature dilute magnetic semiconductor. *Appl. Surf. Sci.* **247**, 493–496 (2005).
14. S. Thota, T. Dutta, and J. Kumar: On the sol–gel synthesis and thermal, structural, and magnetic studies of transition metal (Ni, Co, Mn) containing ZnO powders. *J. Phys. Condens. Matter* **18**, 2473–2486 (2006).
15. S.K. Mandal, A.K. Das, T.K. Nath, D. Karmakar, and B. Satpati: Microstructural and magnetic properties of ZnO:TM (TM = Co, Mn) diluted magnetic semiconducting nanoparticles. *J. Appl. Phys.* **100**, 104315 (2006).
16. K.R. Kittilstved, W.K. Liu, and D.R. Gamelin: Electronic structure origins of polarity-dependent high-TC ferromagnetism in oxide-diluted magnetic semiconductors. *Nat. Mater.* **5**, 291–297 (2006).
17. Q. Wang, Q. Sun, G. Chen, Y. Kawazoe, and P. Jena: Vacancy-induced magnetism in ZnO thin films and nanowires. *Phys. Rev. B* **77**, 205411 (2008).
18. N. Khare, M. J. Kappers, M. Wei, M. G. Blamire, and J. L. MacManus-Driscoll: Defect-induced ferromagnetism in Co-doped ZnO. *Adv. Mater.* **18**(11), 1449–1452 (2006).
19. C. Song, S.N. Pan, X.J. Liu, X.W. Li, F. Zeng, W.S. Yan, B. He, and F. Pan: Evidence of structural defect enhanced room-temperature ferromagnetism in Co-doped ZnO. *J. Phys. Condens. Matter* **19**, 176229 (2007).
20. C.D. Pemmaraju, R. Hanafin, T. Archer, H.B. Braun, and S. Sanvito: Impurity-ion pair induced high-temperature ferromagnetism in Co-doped ZnO. *Phys. Rev. B* **78**, 054428 (2008).
21. M. Berciu and R.N. Bhatt: Effects of disorder on ferromagnetism in diluted magnetic semiconductors. *Phys. Rev. Lett.* **87**, 107203 (2001).
22. J.M.D. Coey, P. Stamenov, R.D. Gunning, M. Venkatesan, and K. Paul: Ferromagnetism in defect-ridden oxides and related materials. *New J. Phys.* **12**, 053025 (2010).
23. D. Chakraborti, G.R. Trichy, J.T. Prater, and J. Narayan: The effect of oxygen annealing on ZnO:Cu and ZnO:(Cu, Al) diluted magnetic semiconductors. *J. Phys. D: Appl. Phys.* **40**, 7606–7613 (2007).
24. S. Bang, S. Lee, J. Park, S. Park, Y. Ko, C. Choi, H. Chang, H. Park, and H. Jeon: The effects of post-annealing on the performance of ZnO thin film transistors. *Thin Solid Films* **519**, 8109–8113 (2011).
25. T. Wang, Y. Liu, Q. Fang, Y. Xuc, G. Li, Z. Sun, M. Wu, J. Li, and H. He: Morphology and optical properties of Co doped ZnO textured thin films. *J. Alloys Compd.* **509**, 9116–9122 (2011).
26. M.M. Can, S.I. Shah, M.F. Doty, C.R. Haughn, and T. Fırat: Electrical and optical properties of point defects in ZnO thin films. *J. Phys. D: Appl. Phys.* **45**, 195104 (2012).
27. M.F. Al-Kuhaili, S.M.A. Durrani, I.A. Bakhtiari, and M. Saleem: Optical constants of vacuum annealed radio frequency (RF) magnetron sputtered zinc oxide thin films. *Opt. Commun.* **285**, 4405–4412 (2012).
28. C. Guillen and J. Herrero: Transparent films on polymers for photovoltaic applications. *Vacuum* **84**, 924–929 (2010).
29. A.K. Srivastava, Praveen, M. Arora, S.K. Gupta, B.R. Chakraborty, S. Chandra, S. Toyoda, and H. Bahadur: Nanostructural features and optical performance of RF magnetron sputtered ZnO thin films. *J. Mater. Sci. Technol.* **26**(11), 986–990 (2010).
30. Y.F. Zhu, G.H. Zhou, H.Y. Ding, A.H. Liu, Y.B. Lin, and Y.W. Dong: Synthesis and characterization of highly-ordered ZnO/PbS core/shell heterostructures. *Superlattices Microstruct.* **50**, 549–556 (2011).
31. A. Layek, B. Manna, and A. Chowdhury: Carrier recombination dynamics through defect states of ZnO nanocrystals: From nanoparticles to nanorods. *Chem. Phys. Lett.* **539–540**, 133–138 (2012).
32. M-W. Ahn, K-S. Park, J-H. Heo, J-G. Park, D-W. Kim, K.J. Choi, J-H. Lee, S-H. Hong: Gas sensing properties of defect-controlled ZnO-nanowire gas sensor. *Appl. Phys. Lett.* **93**, 263103 (2008).
33. H. Jiang, H. Wang, and X. Wang: Facile and mild preparation of fluorescent ZnO nanosheets and their bioimaging applications. *Appl. Surf. Sci.* **257**, 6991–6995 (2011).
34. H-J. Lee, S-Y. Jeong, C.R. Cho, and C.H. Park: Study of diluted magnetic semiconductor: Co-doped ZnO. *Appl. Phys. Lett.* **81**, 4020–4022 (2002).
35. Z. Jin, T. Fukumura, M. Kawasaki, K. Ando, H. Saito, T. Sekiguchi, Y.Z. Yoo, M. Murakami, Y. Matsumoto, T. Hasegawa, and H. Koinuma: High throughput fabrication of transition-metal-doped epitaxial ZnO thin films: A series of oxide-diluted magnetic semiconductors and their properties. *Appl. Phys. Lett.* **78**, 3824–3826 (2001).
36. Y.B. Zhang, Q. Liu, T. Sritharan, C.L. Gan, and S. Li: Pulsed laser ablation of preferentially orientated ZnO:Co diluted magnetic semiconducting thin films on Si substrates. *Appl. Phys. Lett.* **89**, 042510 (2006).
37. Y. Shon, Y.H. Kwon, S.U. Yuldashev, Y.S. Park, D.J. Fu, D.Y. Kim, H.S. Kim, and T.W. Kang: Diluted magnetic semiconductor

of p-type GaN epilayers implanted with Mn^+ ions. *J. Appl. Phys.* **93**, 1546–1548 (2003).
38. K.J. Kim and Y.R. Park: Spectroscopic ellipsometry study of optical transitions in $Zn_{1-x}Co_xO$ alloys. *Appl. Phys. Lett.* **81**, 1420–1422 (2002).
39. S.B. Zhang, S-H. Wei, and A. Zunger: Intrinsic n-type versus p-type doping asymmetry and the defect physics of ZnO. *Phys. Rev. B* **63**, 075205 (2001).
40. C. Ravichandran, G. Srinivasan, C. Lennon, S. Sivananthan, and J. Kumar: Influence of post-deposition annealing on the structural, optical and electrical properties of Li and Mg co-doped ZnO thin films deposited by sol–gel technique. *Superlattices Microstruct.* **49**, 527–536 (2011).
41. B.B. Straumal, S.G. Protasova, A.A. Mazilkin, A.A. Myatiev, P.B. Straumal, G. Schütz, E. Goering, and B. Baretzky: Ferromagnetic properties of the Mn-doped nanograined ZnO films. *J. Appl. Phys.* **108**, 073923 (2010).
42. M. Subramanian, M. Tanemura, T. Hihara, V. Ganesan, T. Soga, and T. Jimbo: Magnetic anisotropy in nanocrystalline Co-doped ZnO thin films. *Chem. Phys. Lett.* **487**, 97–100 (2010).
43. M.M. Can, T. Fırat, and Ş. Özcan: Dominancy of antiferromagnetism in $Zn_{1-x}Co_xO$ diluted magnetic semiconductors. *J. Mater. Sci.* **46**, 1830–1838 (2011).
44. M.M. Can, T. Fırat, and Ş. Özcan: Structural, optic, and magnetic investigation of the synthesized ZnO and $Zn_{0.99}Co_{0.01}O$ semiconductors via solid state reaction. *IEEE Trans. Magn.* **46**(6), 1809–1812 (2010).
45. L. Reimer: *Scanning Electron Microscopy: Physics of Image Formation and Microanalysis* (Springer, Berlin, Germany, 1998); pp. 208–218.
46. J. Husna, M.M. Aliyu, M.A. Islam, P. Chelvanathan, N.R. Hamzah, M.S. Hossain, M.R. Karim, and N. Amin: Influence of annealing temperature on the properties of ZnO thin films grown by sputtering. *Energy Procedia* **25**, 55–61 (2012).
47. P.T. Hsieh, Y.C. Chen, M.S. Lee, K.S. Kao, M.C. Kao, and M.P. Houng: The effects of oxygen concentration on ultraviolet luminescence of ZnO films by sol-gel technology and annealing. *J. Sol-Gel Sci. Technol.* **47**, 1–6 (2008).
48. A.G. Khairnar and A.M. Mahajan: Effect of post-deposition annealing temperature on RF-sputtered HfO_2 thin film for advanced CMOS technology. *Solid State Sci.* **15**, 24–28 (2013).
49. D.R. Sahu and J-L. Huang: The properties of ZnO/Cu/ZnO multilayer films before and after annealing in the different atmosphere. *Thin Solid Films* **516**, 208–211 (2007).
50. C.D. Wagner, W.M. Riggs, L.E. Davis, and J.F. Moulder: *Handbook of X-ray Photoelectron Spectroscopy*, G.E. Muilenberg, ed. (Perkin-Elmer, Minnesota, 1979); pp. 82–83, 88–89, 172–173.
51. L-W. Lai and C-T. Lee: Investigation of optical and electrical properties of ZnO thin films. *Mater. Chem. Phys.* **110**, 393–396 (2008).
52. P-T. Hsieh, Y-C. Chen, K-S. Kao, and C-M. Wang: Luminescence mechanism of ZnO thin film investigated by XPS measurement. *Appl. Phys. A* **90**, 317–321 (2008).
53. S-Y. Sun, J-L. Huang, and D-F. Lii: Effects of oxygen contents on the electrical and optical properties of indium molybdenum oxide films fabricated by high density plasma evaporation. J Vac: *Sci. Technol.* **22**, 1235 (2004).
54. A.J. Fernandes, P.P-T. Chen, M. Wintrebert-Fouquet, H. Timmers, S.K. Shrestha, H. Hirshy, and R.M. Perks, and B.F. Usher: The nature of nitrogen related point defects in common forms of InN. *J. Appl. Phys.* **101**, 123702 (2007).
55. C. Lennon, R.B. Tapia, R. Kodama, Y. Chang, S. Sivananthan, and M. Deshpande: Effects of annealing in a partially reducing atmosphere on sputtered Al-doped ZnO thin films. *J. Electron. Mater.* **38**(8), 1568–1573 (2009).
56. X.L. Xu, S.P. Lau, J.S. Chen, G.Y. Chen, and B.K. Tay: Polycrystalline ZnO thin films on Si (100) deposited by filtered cathodic vacuum arc. *J. Cryst. Growth* **223**, 201–205 (2001).
57. J.N. Zeng, J.K. Low, Z.M. Ren, T. Liew, and Y.F. Lu: Effect of deposition conditions on optical and electrical properties of ZnO films prepared by pulsed laser deposition. *Appl. Surf. Sci.* **197–198**, 362–367 (2002).
58. C. Sudakar, P. Kharel, G. Lawes, R. Suryanarayanan, R. Naik, and V.M. Naik: Raman spectroscopic studies of oxygen defects in Co-doped ZnO films exhibiting room-temperature ferromagnetism. *J. Phys. Condens. Mater.* **19** 026212 (2007).